

α - α Double Folding Cluster Potential Description of the $^{12}\text{C}+^{24}\text{Mg}$ System

M. Karakoc and I. Boztosun

Department of Physics, Erciyes University, Kayseri, Turkey

(Dated: October 29, 2018)

We present a simultaneous analysis of the elastic scattering and fusion cross-section data of the $^{12}\text{C}+^{24}\text{Mg}$ system around the Coulomb barrier and over energies by using the microscopic α - α double folding cluster potential within the framework of the optical model and the coupled-channels formalism. The α - α double folding cluster potential is obtained by using the α -cluster distribution densities of the nuclei in the usual double folding procedure. The microscopic potential results are compared with the findings of the phenomenological deep and shallow potentials. It is subsequently shown that only phenomenological deep real, microscopic nucleon-nucleon and α - α double folding cluster potentials provide a consistent description of the angular distributions and fusion cross-section data simultaneously. The effect of the inclusion of the excited states of the target nucleus ^{24}Mg on the fusion cross-section predictions is also determined by the coupled-channels calculations, which are shown to improve the agreement.

PACS numbers: 24.10.Ht; 24.50.+g; 25.70.-z

Keywords: Optical and coupled-channels models; folding potentials; fusion cross-section; $^{12}\text{C}+^{24}\text{Mg}$ reaction.

I. INTRODUCTION

Determining the shape of the nuclear potential between two colliding pairs is a long-standing problem. The theoretical investigations of the precisely measured experimental data at high energies well over the Coulomb barrier for systems like $^{12}\text{C}+^{12}\text{C}$ and $^{16}\text{O}+^{16}\text{O}$ have led to the determination of the gross features of the local Optical potentials. Subsequently, ambiguities have been clarified in many cases regarding the depths of the real parts of the nuclear potentials [1]. However, it is not yet possible to claim the same conclusive arguments for the shape of the nuclear potential for the reactions around the Coulomb barrier. The theoretical analysis suffers from a number of serious drawbacks such as the failure to determine the shape of the interaction potential, the reproduction of the oscillatory structure and the out-of-phase problem between theoretical predictions and experimental data.

In this context, the $^{12}\text{C}+^{24}\text{Mg}$ reaction [2, 3, 4, 5, 6] has been extensively investigated both experimentally and theoretically. The conventional optical model analysis conducted so far fails to explain all or some of the experimental data by using shallow or deep optical potentials [2, 3, 4]. Moreover, there has been no detailed microscopic study using folding models attempting to explain the individual angular distributions and fusion cross-sections data simultaneously. Therefore, we aim to analyze the $^{12}\text{C}+^{24}\text{Mg}$ system for energies from 16.0 to 24.0 MeV by using the α - α microscopic double folding cluster (DFC) potential. Our results are shown in comparison with the nucleon-nucleon double folding (NN-DF), phenomenological shallow (WS_S) and deep (WS_D^2) real potentials.

In the next section, we introduce the potentials used in the optical model and coupled-channels (CC) formalism. In sections III and IV, the optical and CC results are

shown. Section V is devoted to our conclusion.

II. THE OPTICAL MODEL

In order to make a comparative study of this reaction, we have used four different potentials for the real part of the optical model potential: Two are microscopic, which are calculated from microscopic NN-DF and α - α DFC potentials and the other two are phenomenological deep and shallow potentials. We provide the details of the α - α DFC potential and leave the NN-DF and phenomenological potentials to references provided in [2, 7, 8]. The projectile and target nuclei, which we study in this paper consist of integer multiple of the alpha particles. It has been known that $4n$ type nuclei have an α -cluster structure [9, 10]. Therefore, it will be very interesting to obtain the interaction potential by considering the alpha-particle structure of these nuclei. For this purpose, the α - α DFC potential is constructed in a similar way to the ordinary DF one: We fold an α - α effective interaction with α -clusters distribution densities and formulate the nucleus-nucleus DFC optical model potential [11] as

$$V_{DFC}(r) = \int \int \rho_{cP}(r_1) \rho_{cT}(r_2) \nu_{\alpha\alpha} (|\vec{r} + \vec{r}_2 - \vec{r}_1|) d^3r_1 d^3r_2 \quad (1)$$

where ρ_{cP} and ρ_{cT} are the α -cluster distributions for projectile and target nuclei and $\nu_{\alpha\alpha}$ is the effective α - α interaction.

The matter distribution of a nucleus is known and can be obtained from:

$$\rho_M(r) = \rho_{0M}(1 + wr^2) \exp(-\beta r^2) \quad (2)$$

This is a modified form of the Gaussian shape for the $\rho_M(r)$, projectile and target densities. The matter density of an α nucleus can also be obtained from:

$$\rho_\alpha(r) = \rho_{0\alpha} \exp(-\beta r^2) \quad (3)$$

TABLE I: The parameters of nuclear matter densities of the ^{12}C and ^4He [12]. The parameter of the ^{24}Mg nuclear matter density is obtained from RIPL-2 [13].

Nuclei	ρ_0 (fm^{-3})	w (fm^{-2})	β (fm^{-2})	$\langle r^2 \rangle^{1/2}$ (fm)
^{12}C	0.1644	0.4988	0.3741	2.407
^{24}Mg	0.1499	0.4012	0.2383	3.050
^4He	0.4229	0	0.7024	1.460

The parameters for the $\rho_{0\alpha}$, ρ_{0M} , w and β used in equations 2 and 3 are given in Table I. If $\rho_c(r')$ is the α -cluster distributions function inside the nucleus, then we can relate the nuclear matter density distribution functions of the nucleus, $\rho_M(r)$, to that of the α -particle nucleus, $\rho_\alpha(r)$, as

$$\rho_M(r) = \int \rho_c(r') \rho_\alpha(|\vec{r} - \vec{r}'|) d^3r' \quad (4)$$

Since the densities of the nucleus and the alpha particle can be calculated from equations 2 and 3, by using Fourier transform techniques [14] for expression (4), we can obtain the α -cluster distribution function $\rho_c(r')$ as:

$$\rho_c(r') = \rho_{0c}(1 + \mu r'^2) \exp(-\xi r'^2) \quad (5)$$

with $\eta = \lambda - \beta$, $\xi = \beta\lambda/\eta$, $\mu = \frac{2w\lambda^2}{\eta(2\eta - 3w)}$. Inserting this α -cluster distribution together with the following effective α - α interaction potential of Buck *et al.* [15], we can obtain the α - α DFC from equation 1.

$$\nu_{\alpha\alpha}(r) = -122.6225 \exp(-0.22r^2) \quad (6)$$

For the phenomenological potentials, we use slightly modified versions of the potentials previously conducted for this reaction. For the deep potential, we use the potentials of Boztosun and Rae [6] and for the shallow potential, we use the potentials of Sciani *et al* [2].

The parameters of the potentials are given in Table II. The codes Dfpot [16] and Fresco [17] are used for all calculations.

III. RESULTS AND DISCUSSIONS

The experimental data of the $^{12}\text{C}+^{24}\text{Mg}$ reaction has been analyzed in the laboratory system from 16.0 to 24.0 MeV by using both phenomenological and microscopic potentials within the above-described optical model.

In order to obtain the best fit between the experimental data and the theoretical calculations, we have conducted a χ^2 search to define the parameters of the potentials. For the microscopic DF potentials, we have two free parameters: N_R and W_0 . The normalization factor (N_R) of the real part and the depth (W_0) of the imaginary part have been varied on a grid and the results of this systematic search have shown that the N_R or W_0 parameters

TABLE II: The parameters of the real and imaginary potentials. All imaginary potentials have WS volume shape.

Pot. Type	V_0 (MeV)	r_V (fm)	a_V (fm)	W_0 (MeV)	r_W (fm)	a_W (fm)
NN	-	-	-	$1.8E + 1.6$	0.30	0.286
α - α	-	-	-	$3.7E - 43.4$	0.30	0.286
WS_D^2	427.0	0.88	1.187	$0.4E + 30.0$	0.30	0.286
WS_S	$49.1 - 0.56E$	1.29	0.400	$0.054E - 0.47$	1.77	0.600

TABLE III: Theoretical reaction and experimental fusion cross-sections. Experimental data are taken from [18, 19].

E (MeV)	σ (mb)				
	Exp.	NN-DF	α - α DFC	WS_D^2	WS_S
20.0	198.82	243.23	273.66	236.11	432.50
21.0	243.56	320.64	354.45	311.83	530.18
22.0	331.73	393.56	430.47	371.41	678.13
23.0	426.43	456.69	493.40	443.54	723.56
24.0	435.01	518.43	553.70	493.81	791.99

cannot be varied continuously and still produce equally satisfying fits. For the normalization factor of α - α DFC potential, the lowest χ^2 values are generally obtained between 0.7 and 0.9, but we have chosen the parameter $N_{R\alpha-\alpha}=0.72$, which provides a consistent description for all energies. For the NN-DF potential, $N_{R_{NN}}=0.84$.

Some of the results of our analysis obtained by using microscopic and phenomenological potentials are shown in Figure 1 for the individual angular distributions and in Figure 2 for the fusion cross-section data. Numerical values at energies where the experimental data are available, are also shown in Table III for the fusion cross-section.

We may infer from the figures that the theoretical results obtained by using the microscopic and phenomenological potentials present more or less the same behavior: It is difficult to see the difference at forward angles since they overlap. The difference becomes apparent at large angles. However, the lowest χ^2 values for the individual angular distributions are provided by the shallow real potential. If we perceive the lowest χ^2 values as the best fit, then we may say that the shallow potential provides the best fit. If we look at the figures, we also perceive that the theoretical results obtained by using the shallow potential give very good agreement with the experimental data at forward, intermediate and large angles. The magnitude of the cross-section is correctly provided and the minima/maxima are at the correct places with phases.

However, the same shallow potential that explains the angular distribution is unable to predict the fusion cross-section. The theoretical calculation for the fusion cross-section is almost twice as big as the experimental data.

Nevertheless, the deep potentials, both microscopic and phenomenological ones, provide a good agreement for the individual angular distributions with acceptable χ^2 values and predict the fusion cross-section reasonably well. The magnitude of the cross-section is correctly pre-

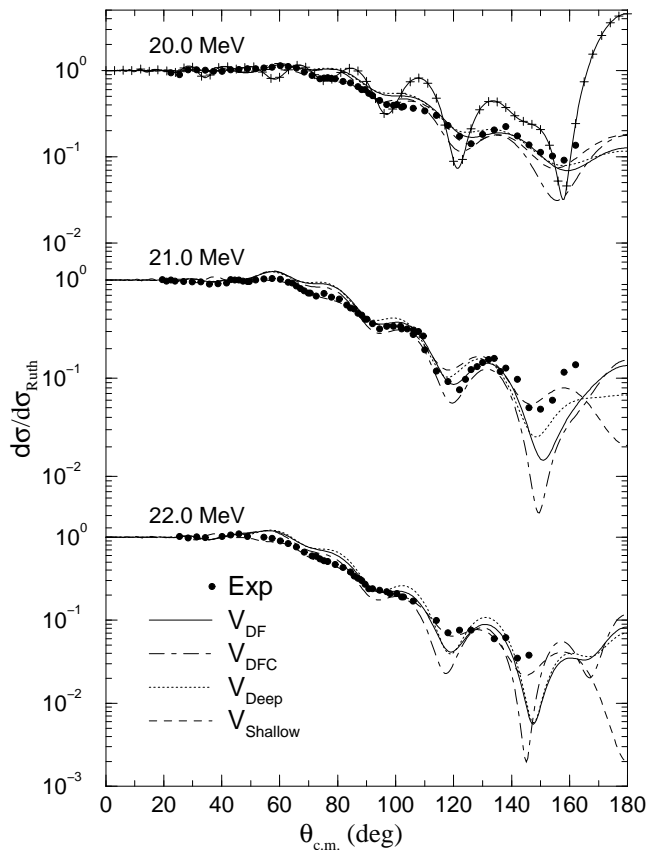


FIG. 1: OM elastic scattering results obtained by using NN-DF (solid lines), α - α DFC (dot dashed lines), phenomenological deep (dotted lines) and shallow (dashed lines) potentials. The solid line with plus shows the CC prediction of the shallow potential using the short range imaginary potential at $E_{Lab}=20\text{MeV}$ (see the text). Experimental data is from [2].

dicted and the minima/maxima are at the correct places with phases. The only discrepancy is at large angles where minima are predicted deeper than the measured data.

IV. COUPLED-CHANNELS CALCULATIONS

The optical model calculations in the previous section provide the total reaction cross-section, but not the fusion, therefore, there is a discrepancy between theoretical predictions and the experimental fusion cross-section data. In order to obtain the fusion cross-section and improve the agreement, we have to either use a model-independent approach such as the one used by references [20, 21] or remove the non-elastic cross-section from reaction cross-section calculations; we have used the CC model for this purpose and in our calculations, the fusion cross-section is obtained in the following way:

$$\sigma_F = \sigma_R - \sigma_{in} \quad (7)$$

where σ_F denotes the fusion, σ_R is the total reaction and σ_{in} , the non-elastic cross-sections. In the present CC

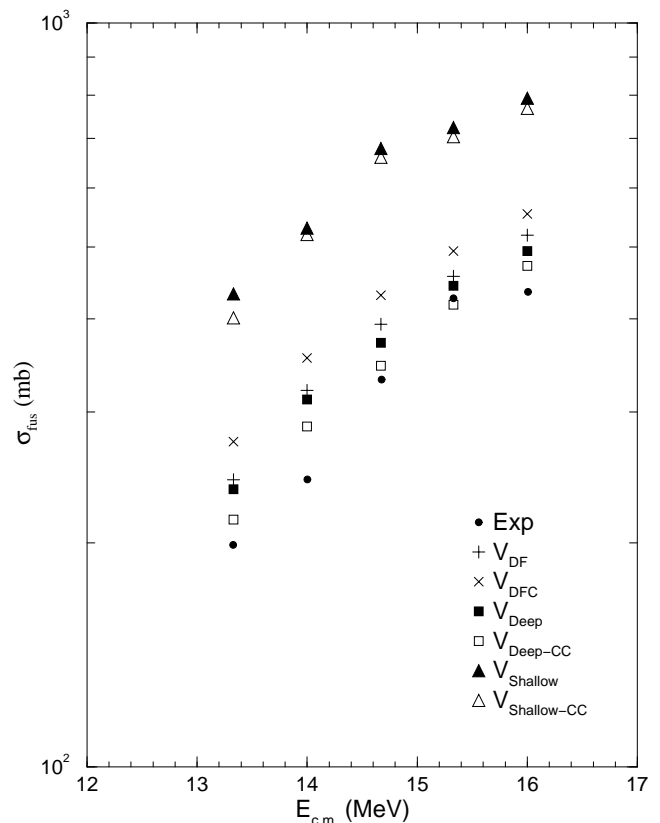


FIG. 2: Experimental fusion cross-sections (filled circles) [18, 19] are compared with theoretically calculated results using the NN-DF (plus), the α - α DFC (cross), phenomenological deep (filled squares) and shallow (filled triangle-up) potentials. The coupled channels calculation results using the phenomenological deep (squares) and shallow (triangle-up) potentials are also shown.

calculations, we describe the interaction between ^{12}C and ^{24}Mg nuclei with a deformed optical potential. The real potential is assumed to have the square of a Woods-Saxon and the imaginary potential has the standard Woods-Saxon volume shape [6].

We assume that the target nucleus ^{24}Mg has a static quadrupole deformation, and that its rotation can be described within the framework of the rotational model by deforming the real potential in the following way

$$R(\theta, \phi) = r_0 A_p^{1/3} + r_0 A_t^{1/3} [1 + \beta_2 Y_{20}(\theta, \phi)] \quad (8)$$

where p and t refer to projectile and target nuclei respectively and β_2 is the deformation parameter of ^{24}Mg . We shall use the exact value of β_2 , derived from the deformation length $\delta=1.50\text{ fm}$ ($\beta=0.52$). For the Coulomb deformation, we assume $\beta_2^C = \beta_2^N$.

The results of the CC calculations are shown in Figure 2 and in Table IV for the fusion calculations. We do not show the elastic scattering angular distribution results obtained since we are mainly interested in the effect of the CC calculation on the fusion data prediction. Nevertheless, the CC results for the elastic scattering angular distribution are reasonably well. From Figure 2,

TABLE IV: Comparison of the CC and optical model (OM) fusion cross-section predictions using deep (D) and shallow (S) potentials. Experimental data are from [18, 19].

E (MeV)	Exp.	$\sigma(mb)$					
		σ_{OM_D}		σ_{CC_D}		σ_{OM_S}	
		σ_F	σ_{2+}	σ_F	σ_{2+}	σ_F	σ_{2+}
20.0	198.82	236.11	215.08	22.85	432.50	401.49	26.80
21.0	243.56	311.83	286.72	27.10	530.18	519.42	31.64
22.0	331.73	371.41	346.04	29.86	678.13	659.74	31.71
23.0	426.43	443.54	418.00	32.33	723.56	703.22	39.64
24.0	435.01	493.81	471.67	34.10	791.99	767.74	45.05

it is clear that the inclusion of the 2^+ and 4^+ excited states of ^{24}Mg affects the calculations and gives a better agreement for the fusion calculations in comparison with the optical model. The numerical values of this effect can be seen from Table IV. In this table, we present the optical and CC results for the deep Woods-Saxon squared phenomenological and shallow Woods-Saxon volume potentials. The inclusion of the 2^+ and 4^+ excited states of ^{24}Mg removes flux from the elastic channel and the CC results for the fusion data are in better agreement than the optical model one. From Table IV, it may be observed that, while the optical model prediction is around $\sigma_F=236.11\text{mb}$ at $E_{Lab}=20.0$ MeV, it becomes $\sigma_F=215.08\text{mb}$ after the inclusion of the 2^+ and 4^+ excited states of ^{24}Mg . The effect is around 22.85mb , which makes the theoretical CC prediction better in agreement with the experimental data. The same effect has been also observed for the shallow real potential, the coupled-channel calculations improve the agreement with the experimental fusion data, but it is still far from being comparable with the prediction of the deep potentials.

We have noticed that the failure of the shallow potential may be related to the long-range imaginary potential we have used in the calculations. Because of this long range imaginary potential, we cannot obtain satisfactory agreement with the fusion cross-section. However, when we reduce the range of the imaginary potential and use

the one similar to the deep potential model, we get a better agreement with the fusion data, but this time we are unable to obtain a good agreement with the elastic scattering angular distribution. This is illustrated in Figure 1 at $E_{Lab}=20.0$ MeV. In this figure, the solid line with plus shows the prediction of a short ranged imaginary potential as used in the deep Woods-Saxon squared potential. The parameters are given in Table II. As a result, we have reached the conclusion that it is not possible to explain the elastic scattering angular distribution and fusion cross-section simultaneously by using a shallow real potential in contrast with the deep one.

V. SUMMARY AND CONCLUSION

The theoretical description of the $^{12}\text{C}+^{24}\text{Mg}$ system has been very difficult since the experimental data show very oscillatory features near the Coulomb barrier at very low energies and a striking backward rise and oscillatory features at forward, intermediate and backward angles at high energies. In this paper, we have shown a consistent description of the elastic scattering of the $^{12}\text{C}+^{24}\text{Mg}$ system at energies around the Coulomb barrier and over, from 16.0 MeV to 24.0 MeV, in the laboratory system by using the NN-DF and α - α DFC potentials in the Optical model calculations. This constitutes the first detailed application of the folding model. All potentials, both deep and shallow, have provided excellent agreement with the experimental data for the elastic scattering individual angular distributions at different laboratory energies; however, only deep potentials explain the angular distributions and fusion cross-section data simultaneously. As we have argued in the paper, the origin of the large difference between deep and shallow potentials for the fusion cross-section data is related to the long-range imaginary potential. This work clearly demonstrates the inadequacy of using shallow potentials in describing such nuclear reactions and underlines the validity of the double folding potentials.

This project is supported by TÜBİTAK, Grant No: TBAG-2398 and Erciyes University, FBT-04-15.

-
- [1] M.E. Brandan, G.R. Satchler, Phys. Rep. 285 (1997) 143.
[2] W. Sciani, A. Lepine-Szily, F.R. Lichtenthaler, P. Fachine, L.C. Gomes, G.F. Lima, M.M. Obuti, J.M. Jr Oliveira and A.C.C. Villari, Nucl. Phys. **A620**, 91 (1997).
[3] A. Lepine-Szily, W. Sciani, Y.K. Watari, W. Mittag, F.R. Lichtenthaler, M.M. Obuti, J.M. Jr Oliveira and A.C.C. Villari, Phys. Lett. **B304**, 45 (1993).
[4] R.L. Filho, A. Lpine-Szily, A.C.C. Villari and O.P. Filho, Phys. Rev. C **39** (1989) 884.
[5] J. Carter, R.G. Clarkson, V. Hnizdo, R.J. Keddy, D.W. Mingay, F. Osterfeld and J.P.F. Sellschop, Nucl. Phys. **A273**, 523 (1976).
[6] I. Boztosun, W.D.M. Rae, Phys. Rev. **C64** 054607 (2001).
[7] S. Erturk, I. Boztosun, Y. Kucuk, M. Karakoc and S. Aydin, J. Phys. G **31** (2005) S1837.
[8] M. Karakoc, MSc Thesis, Erciyes University (2005).
[9] W.D.M. Rae, Int. J. of Mod. Phys. A. **3** (1988) 1343.
[10] M. Freer, A.C. Merchant, J. Phys. **G23** (1997) 261.
[11] M. El-Azab Farid, Z. M. M. Mahmoud and G. S. Hassan, Nucl. Phys. **A691** (2001) 671.
[12] M. El-Azab Farid, M. A. Hassanain, Nucl. Phys. **A678** (2000) 39.
[13] RIPL-2, Nuclear Matter Densities, IAEA, <http://www-nds.iaea.org/RIPL-2/>
[14] G.R. Satchler, W.G. Love, Phys. Rep. 55 (1979) 183.
[15] Buck, H. Friedrich and C. Wuehly Nucl. Phys. **A275** (1977) 246.
[16] J. Cook, Comput. Phys. Commun., 25 (1982) 125.
[17] I.J. Thompson, FRESKO, CC code, unpublished.
[18] A. Iwamoto, P. Moeller, J.R. Nix and H. Sagawa, Nucl.

Phys. **A506** (1996) 329.

[19] S. Gary, C. Volant, Phys. Rev. C **25**, 1877 (1982).

[20] J.T. Holdeman, R.M. Thaler, Phys. Rev. Lett.**14** (1965)

81; *ibid*, Phys. Rev.**139** B1186 (1965).

[21] T. Yamaya *et al.*, Phys. Lett.**B417** (1998) 7.